High-Resolution Sea Surface Temperature Retrieval from Landsat 8 OLI/TIRS Data at Coastal Region

Kyung-Ae Park[1] and Jae-Cheol Jang[2]

[1] Department of Earth Science Education, Seoul National University, Seoul, Republic of Korea
[2] Department of Science Education, Seoul National University, Seoul, Republic of Korea

Abstract

High-resolution sea surface temperature (SST) images are essential to study the highly variable small-scale oceanic phenomena in the coastal region. Most of the previous SST algorithms are focused on the low or medium resolution SST from the near polar orbiting or geostationary satellites. The Landsat 8 Operational Land Imager and Thermal Infrared Sensor (OLI/TIRS) makes it possible to obtain high-resolution SST images of the coastal regions. This study performed a matchup procedure between 276 Landsat-8 images and in situ temperature measurements of buoys off the coast of the Korean Peninsula from April 2013 to August 2017. Using the matchup database, we investigated SST errors for each formulation of the Multi-Channel SST (MCSST) and the Non-Linear SST (NLSST) by considering the satellite zenith angle (SZA) and the first-guess SST. The retrieved SST equations showed RMS errors from 0.59 °C to 0.72 °C. Smallest errors were found for the NLSST equation that considers the SZA and uses the first-guess SST, compared with the MCSST equations. The SST errors showed characteristic dependences on the atmospheric water vapor, the SZA, and the wind speed. In spite of the narrow swath width of the Landsat-8, the effect of the SZA on the errors was estimated to be significant and considerable for all the formations. Although the coefficients were calculated in the coastal regions around the Korean Peninsula, these coefficients are expected to be feasible for SST retrieval applied to any other parts of the global ocean. This study also addressed the need for high-resolution, coastal SST, by emphasizing the usefulness of the high-resolution Landsat 8 OLI/TIRS data for monitoring the small-scale oceanic phenomena in the coastal regions.

Study Area and Data

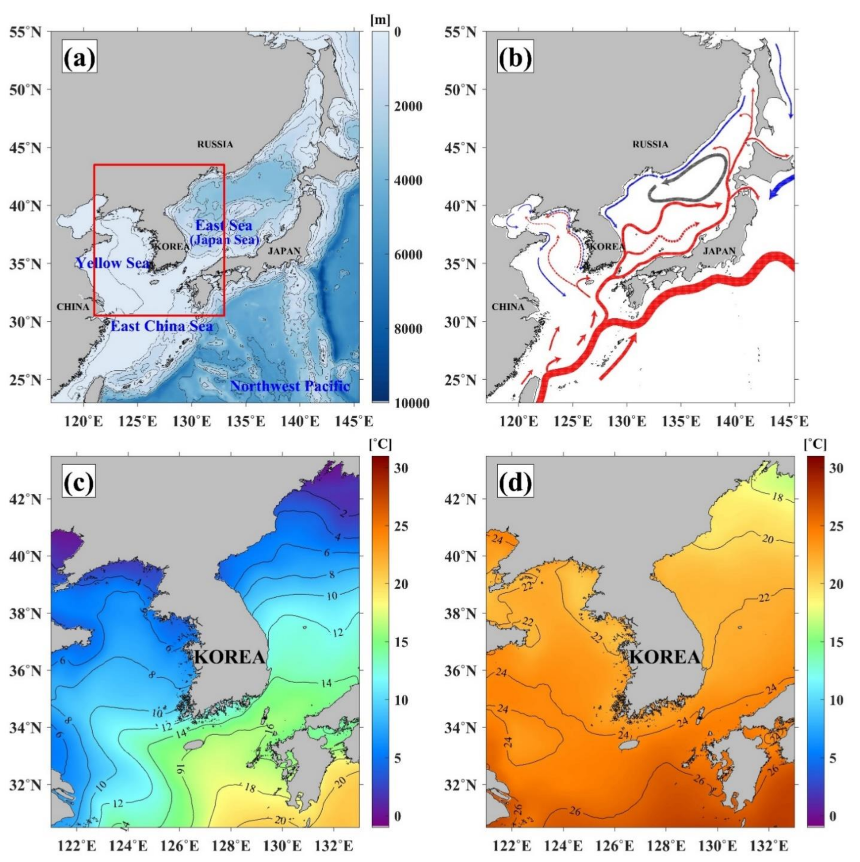

◀ **Figure 1.** . (a) Location of the study area with contours of the water depth (m) in the seas around the Northeast Asia including China, Japan, Korea, and Russia, which red box indicates the study area, (b) a schematic current map with cold (blue) and warm (red) currents (Park et al., 2013), and monthly mean of climatology SST (°C) in the study area from 2002 to 2015 in (c) winter (January) and (d) summer (July).

▪ Buoy Stations

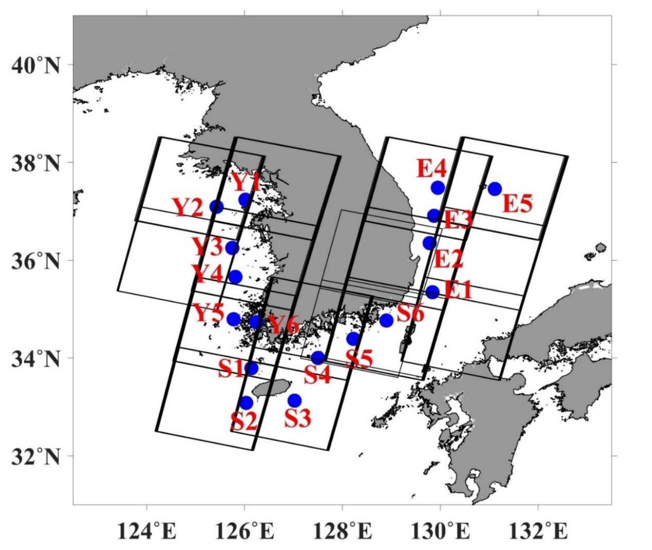

▲ **Figure 2.** Distribution (black boxes) of the Landsat 8 OLI/TIRS images including the Korea Meteorological Administration (KMA) marine meteorological buoys from April 1, 2013 to August 31, 2017, where the blue circles and the red text around the circles indicate the location and symbol of the KMA marine meteorological buoys, respectively.

Table 1. Marine meteorological buoy station specification of Korea Meteorological Administration (KMA) in the seas around the Korean Peninsula including the measurement heights of wind speed and sea temperature.

Ocean	Station		Location		Observation Height (m)		Date of Installation
	Symbol	Name	Longitude	Latitude	Wind Speed	Sea Temp.	
Yellow Sea	Y1	Deokjeokdo	126°01`08``E	37°14`10``N	3.6	0.2	Jul. 1996
	Y2	Incheon	125°25`44``E	37°05`30``N	3.6	0.2	Dec. 2015
	Y3	Oeyeondo	125°45`00``E	36°15`00``N	3.6	0.2	Nov. 2009
	Y4	Buan	125°48`50``E	35°39`31``N	3.6	0.2	Dec. 2015
	Y5	Chilbaldo	125°46`37``E	34°47`36``N	3.6	0.2	Jul. 1996
	Y6	Shinan	126°14`30``E	34°44`00``N	3.6	0.2	Jun. 2013
Southern region	S1	Chujado	126°08`28``E	33°47`37``N	4.0	0.1	Jan. 2014
	S2	Marado	126°02`00``E	33°05`00``N	3.9	0.4	Nov. 2008
	S3	Seogwipo	127°01`22``E	33°07`41``N	3.6	0.4	Dec. 2015
	S4	Geomundo	127°30`05``E	34°00`05``N	3.6	0.2	May 1997
	S5	Tongyeong	128°13`30``E	34°23`30``N	3.6	0.2	Dec. 2015
	S6	Geojedo	128°54`00``E	34°46`00``N	3.6	0.2	1998. 05.
East Sea/ Japan Sea	E1	Ulsan	129°50`29``E	35°20`43``N	3.6	0.4	Dec. 2015
	E2	Pohang	129°47`00``E	36°21`00``N	3.9	0.4	Nov. 2008
	E3	Uljin	129°52`28``E	36°54`25``N	3.6	0.4	Dec. 2015
	E4	Donghae	129°57`00``E	37°28`50``N	3.9	0.4	May 2001
	E5	Ulleungdo	131°06`52``E	37°27`20``N	3.9	0.4	Dec. 2011

Daily SST:. For estimating the coefficients using the NLSST formulation, the first-guess SST is needed and can be obtained from the estimated MCSST or climatological SST. This study used the Operational Sea Surface Temperature and Sea Ice Analysis (OSTIA) data provided by the Met Office with 6 km spatial resolution and the Multi-scale Ultra-high Resolution SST (MURSST) data with 1 km spatial resolution, as the first-guess SST data.

Methods

Satellite Zenith Angle

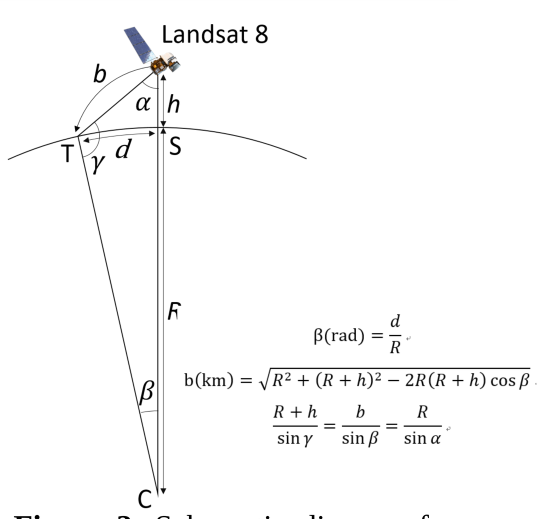

▲ **Figure 3.** Schematic diagram for geographic definition relating the along-scan distance d to the viewing angle α. (C is the center of the Earth, S is the sub-satellite point, and T is the location of target pixel. R is the radius of the Earth and h is the satellite altitude)

Cloud Removal

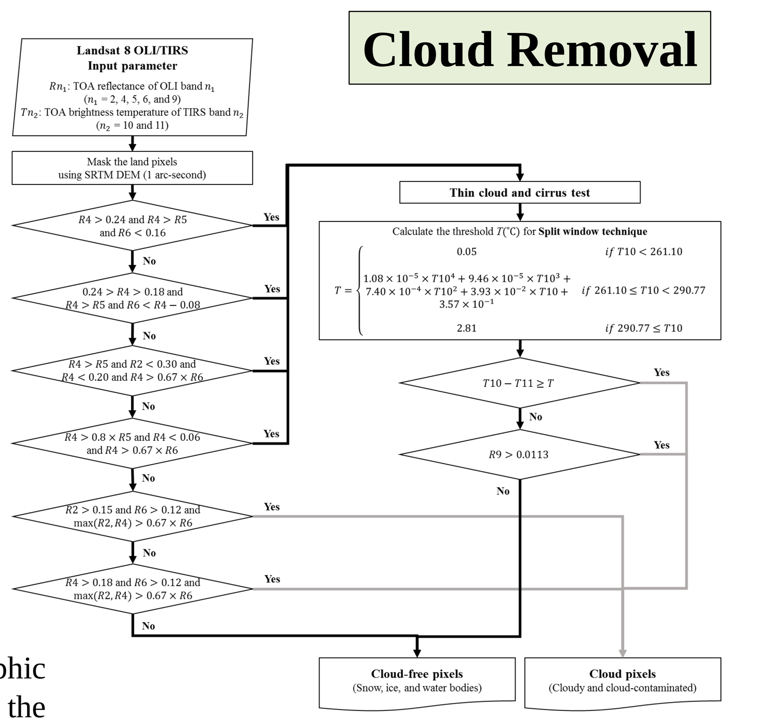

▲ **Figure 4.** Flow chart of the pixel classification algorithm into the cloud-free pixels, including snow, ice, and water bodies, and cloud pixels, including cloudy and cloud-contaminated.

SST retrieval algorithms

Table 2. Formula based on MCSST and NLSST algorithms (T11 and T12: Brightness temperature at 11 μm and 12 μm (in Celsius), Tsfc1, Tsfc2, and Tsfc3: MCSST, OSTIA SST, and MURSST as first-guess SST (in Celsius), θ: satellite zenith angle, $a1$, $a2$, $a3$, and $a4$: regression coefficients).

Algorithm	Number	Equation
MCSST	MCSST1	$SST = a_1T_{11} + a_2(T_{11} - T_{12}) + a_3$
	MCSST2	$SST = a_1T_{11} + a_2(T_{11} - T_{12}) + a_3(T_{11} - T_{12})(\sec\theta - 1) + a_4$
NLSST	NLSST1	$SST = a_1T_{11} + a_2T_{sfc1}(T_{11} - T_{12}) + a_3$
	NLSST2	$SST = a_1T_{11} + a_2T_{sfc2}(T_{11} - T_{12}) + a_3$
	NLSST3	$SST = a_1T_{11} + a_2T_{sfc3}(T_{11} - T_{12}) + a_3$
	NLSST4	$SST = a_1T_{11} + a_2T_{sfc1}(T_{11} - T_{12}) + a_3(T_{11} - T_{12})(\sec\theta - 1) + a_4$
	NLSST5	$SST = a_1T_{11} + a_2T_{sfc2}(T_{11} - T_{12}) + a_3(T_{11} - T_{12})(\sec\theta - 1) + a_4$
	NLSST6	$SST = a_1T_{11} + a_2T_{sfc3}(T_{11} - T_{12}) + a_3(T_{11} - T_{12})(\sec\theta - 1) + a_4$

Quality Control

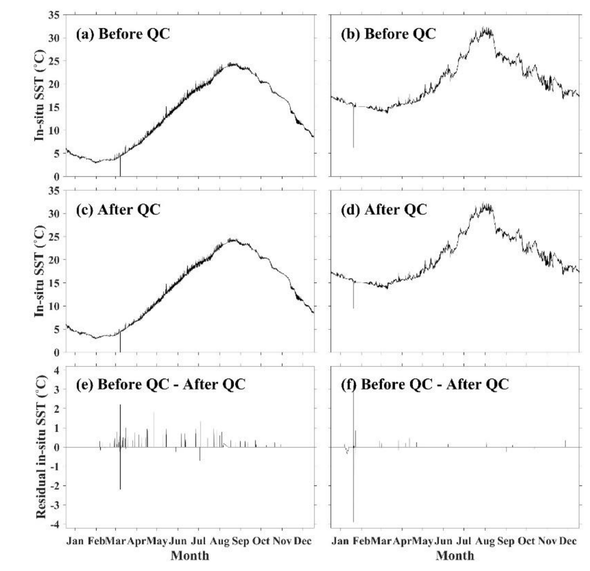

◀ **Figure 5.** Examples of time series of in-situ sea temperature (°C) observed by KMA buoys (a, b) before and (c, d) after QC procedure to remove abnormal temperatures and (e, f) the comparison of residual (before QC procedure – after QC procedure).

- Sequential tests to remove low-quality data and outliers; At least 10 measurements within a day; The maximum and minimum SST difference within a day less than 4 °C. For the time-continuity test, the difference of SST from the daily mean should be less than three standard deviations of the temperatures within 1 day and 4 days. The standard deviation of SST within 4 days should be less than 2 °C.

Matchup Data

Temporal Variation and Matchup

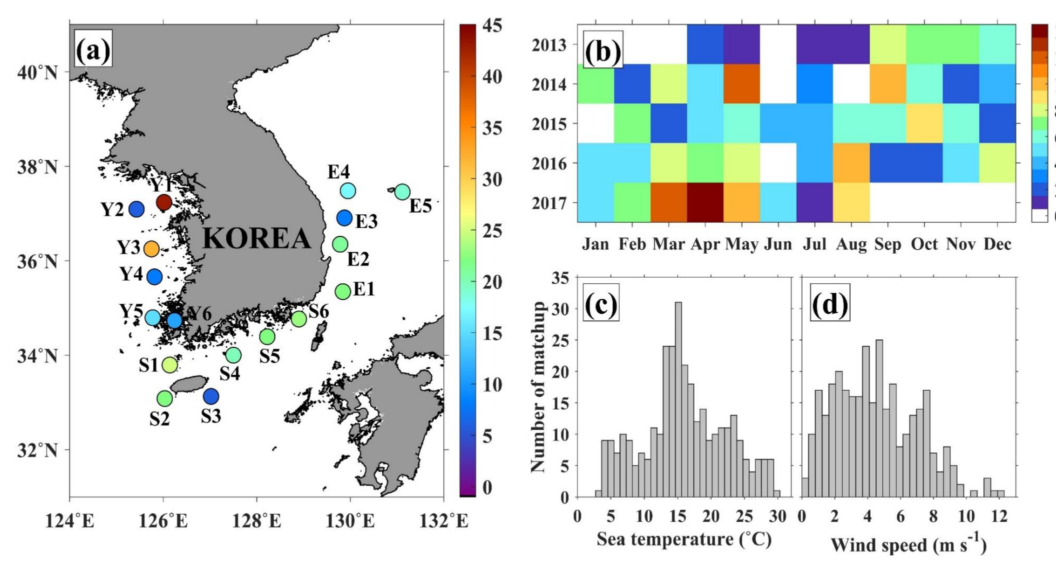

▲ **Figure 6.** (a) The number of the matchup data for each KMA marine meteorological buoys in the seas around the Korean Peninsula, (b) the number of the Landsat 8 OLI/TIRS image acquisition from April 1, 2013 to August 31, 2017, and the histograms of the matchup data with respect to (c) sea temperature and (d) wind speed

Derivation of SST Coefficients

Table 3. Coefficients of MCSST1, MCSST2, NLSST1, NLSST2, NLSST3, NLSST4, NLSST5, and NLSST6 algorithms and root-mean-square error (RMSE) and bias error.

Algorithm	Number	Coefficients				RMSE (°C)	Bias (°C)
		a_1	a_2	a_3	a_4		
MCSST	MCSST1	0.9767	1.8362	0.0699		0.7214	-2.0428E-15
	MCSST2	0.9742	1.7742	32.9868	0.0637	0.7103	-3.5472E15
NLSST	NLSST1	0.9042	0.0824	1.4408		0.6661	1.2879E-15
	NLSST2	0.8965	0.0842	1.5122		0.6110	3.7748E-16
	NLSST3	0.9009	0.0817	1.4808		0.6352	1.4710E-15
	NLSST4	0.9026	0.0802	32.0333	1.3990	0.6514	3.3973E-15
	NLSST5	0.8953	0.0819	32.3713	1.4672	0.5982	1.1047E-15
	NLSST6	0.8992	0.0793	35.3699	1.4341	0.6205	1.7764E-15

Comparison of Landsat-8 SST and In-situ Temp.

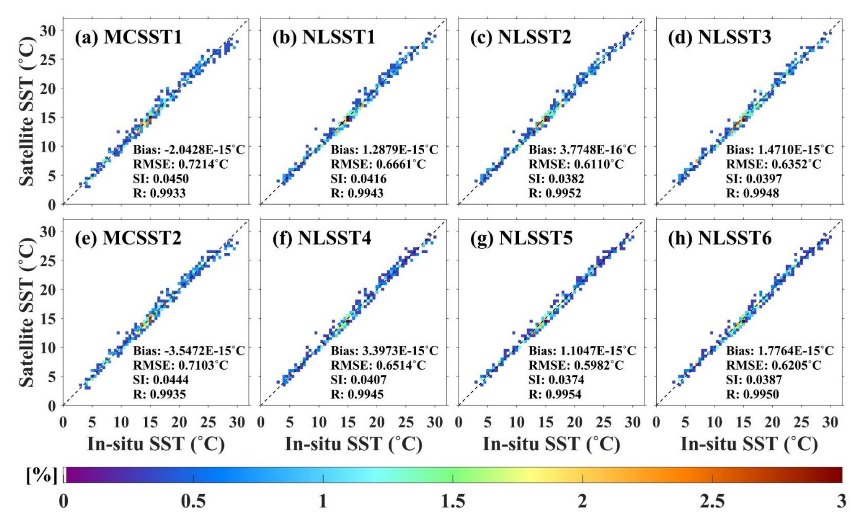

▲ **Figure 7.** Comparison between satellite derived SST and in-situ temperature using (a, e) MCSST and (b, c, d, f, g, h) NLSST algorithms, where the color represents the percentage of the data to the total number of matchup points in a bin of 0.5°C x 0.5°C. Bias, root-mean-square error (RMSE), scatter index (SI), and correlation coefficient (R) are given in each plot.

High-resolution SST

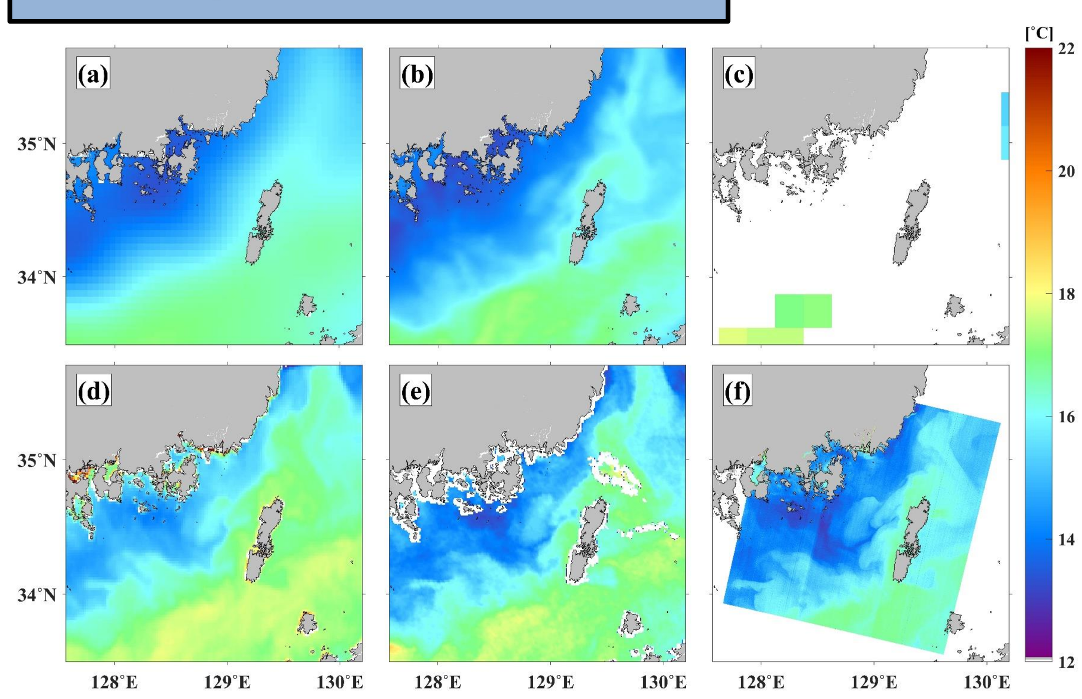

The Landsat 8 has an exceptionally high spatial resolution compared with other satellites used for SST retrieval. Due to its low spatial resolution of AMSR-2 of about 25 km and the effect of land on microwave measurements, there were only a few pixels with SSTs without any observations in the coastal area from 50 km to 100 km distance from the shoreline. On the contrary, the Himawari-8/AHI produced SSTs with relatively high spatial resolution of about 2 km. The NOAA/AVHRR data with a spatial resolution of about 1.1 km revealed more detailed structure of SST distribution including the contrast differences of temperatures at the frontal region between the onshore and the offshore regions. Coastal SST patterns of the Landsat 8 (Figure 8f) illustrated detailed spatial structures as compared with those from other SST products (Figure 8a-e). This demonstrated the capability and usefulness of Landsat-8 data at the coastal regions including the estuarine regions.

◀ **Figure 8.** Distributions of SST derived from (a) OSTIA SST daily composite on 19 April 2016, (b) MURSST daily composite on 19 April 2016, (c) GCOM/W1 AMSR-2 observed at 05 UTC on 19 April 2016, (d) Himawari-8 AHI observed at 02 UTC on 19 April 2016, (e) NOAA-19 AVHRR observed at 05 UTC on 19 April 2016, and (f) Landsat 8 OLI/TIRS observed at 02 UTC on 19 April 2016 using NLSST4 algorithm.

Effect of Atmospheric Moisture

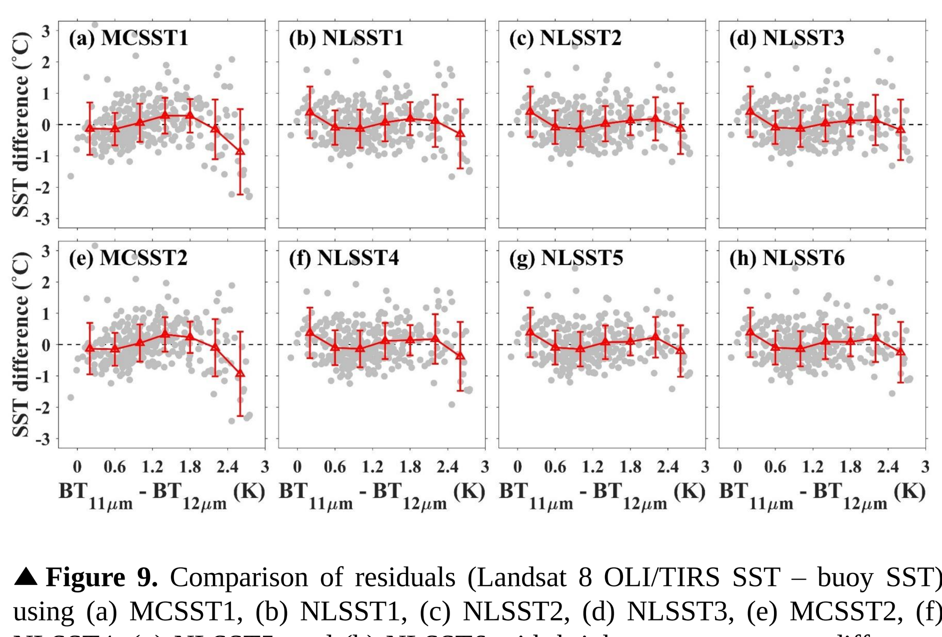

▲ **Figure 9.** Comparison of residuals (Landsat 8 OLI/TIRS SST – buoy SST) using (a) MCSST1, (b) NLSST1, (c) NLSST2, (d) NLSST3, (e) MCSST2, (f) NLSST4, (g) NLSST5, and (h) NLSST6 with brightness temperature difference between 11 μm and 12 μm, where the red points and bars represent the mean value and standard deviation of SST errors for each interval, respectively.

Effect of Satelite Zenith Angle

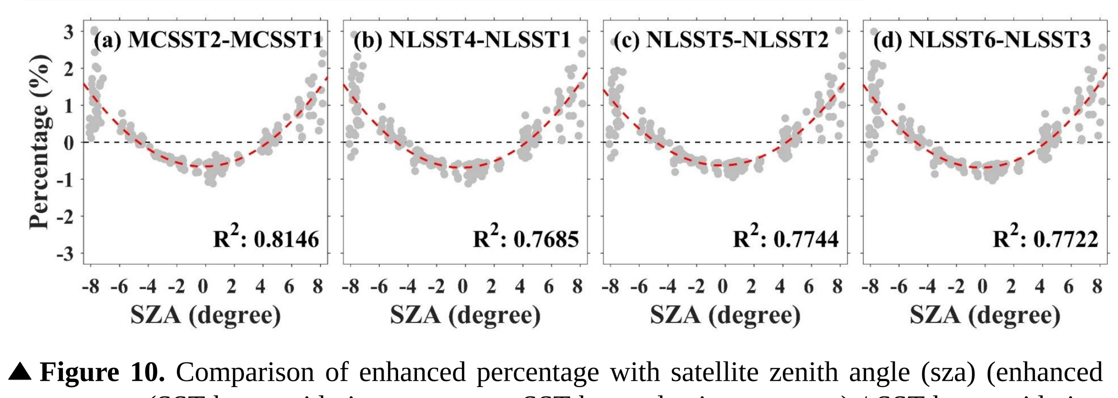

▲ **Figure 10.** Comparison of enhanced percentage with satellite zenith angle (sza) (enhanced percentage: (SST by considering sza term – SST by neglecting sza term) / SST by considering sza term) using (a) MCSST2 and MCSST1, (b) NLSST4 and NLSST1, (c) NLSST5 and NLSST2, and (d) NLSST6 and NLSST3, where the red dashed lines represent the 2nd order polynomial fitted lines.

The maximum decrease was 0.75% in the range from -1 to 1 degree, and the maximum increase was 1.49% in the range from 7 to 9 degree. By adding the SZA term, the estimated SST was improved in the opposite direction based on ±4 degrees, resulting in an increase of about 0.1 °C in RMSE. The accuracies of the SSTs on the edges with high SZA of about -8 or 8 degrees improved over 1% by reaching 3%. Other cases of the NLSST formulations also revealed improved capability of the algorithms in reducing the errors when the SST formulations included the SZA term. This implies that the SST formulation should include the SZA to estimate more accurate SST from the Landsat-8 data in spite of its narrow swath width.

Atmospheric Imprint

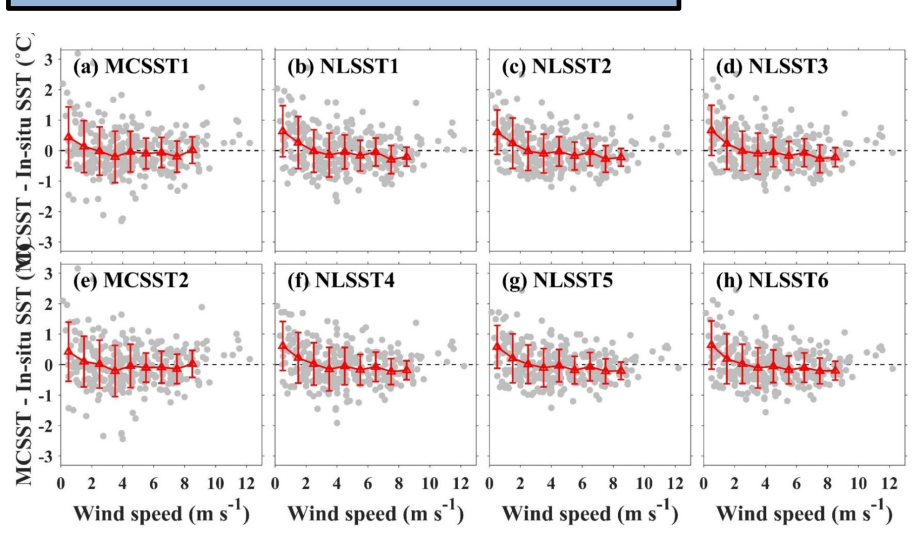

▲ **Figure 11.** Comparison of residuals (Landsat 8 OLI/TIRS SST – buoy SST) using (a) MCSST1, (b) NLSST1, (c) NLSST2, (d) NLSST3, (e) MCSST2, (f) NLSST4, (g) NLSST5, and (h) NLSST6 with wind speed, where the red points and bars represent the mean value and standard deviation of SST errors for each interval, respectively.

Conclusion

- A total number of 276 Landsat 8 OLI/TIRS images 11μm and 12μm bands were used to produce 320 matchup data for the period from April 2013 to August 2017. The RMSE ranged from 0.59 K to 0.72K depending on SST algorithms. SST errors were greatly reduced in the case of the NLSST formulations by applying the SZA and the use of the proper first-guess SST.
- The satellite-derived MCSSTs had a tendency to be underestimated at relatively high moist condition of greater than 2 K. The SST errors revealed the quadratic dependence on the SZA values from the nadir to the edge of the swath. The inclusion of SZA term in the SST estimation moderately improved by less than 3% as compared with prior equations without the angle term. The SST errors were amplified as the wind speeds became weak at a range of less than 2 m s^{-1}.
- When the SST coefficients calculated from the matchup data from April 2013 to August 2016 were applied to the data from September 2016 to August 2017, the RMSE was less than about 0.7 K. The SST coefficients derived in this study might be applicable to SST derivation for other coastal regions of the global ocean as well, especially for the regions without any local SST coefficients for the Landsat-8 data. For more extensive and operational use of the Landsat 8 OLI/TIRS derived SSTs, it is important to continuously monitor and understand the error characteristics of the SST using in-situ measurements in diverse ocean regions. It is expected that the present SST algorithms and coefficients could be further improved in the future and be extensively used for studying small-scale ocean phenomena in the coastal regions including estuarine regions.